Defence Technology 13 (2017) 158–163

Contents lists available at ScienceDirect

Defence Technology

journal homepage: www.elsevier.com/locate/dt

Trajectory optimization of a deflectable nose missile

Zhi-yong Zhang [a], Qi-zhong Tang [b], Xiao-hui Sun [a, *], Zhi-hua Chen [a]

[a] National Key Laboratory of Transient Physics, Nanjing University of Science and Technology, Nanjing 210094, China
[b] North China System Engineering Institute, Beijing 100089, China

ARTICLE INFO

Article history:
Received 18 December 2016
Received in revised form
3 May 2017
Accepted 10 May 2017
Available online 10 May 2017

Keywords:
Deflectable nose missile
Numerical simulation
Maximum range
Maneuverability
Genetic algorithm

ABSTRACT

The deflectable nose missile has a longer range by deflecting its nose to improve its aerodynamic feature. Based on detached eddy simulation (DES), the supersonic flow fields of a missile with deflectable nose are simulated numerically and its aerodynamic force coefficients are calculated under the condition of the deflection angles vary from 0° to 8°, angles of attack, 0°–8°, and mach numbers, 2 to 5. Coupling these aerodynamic coefficients with the plumb plane ballistic equations, the extended flight range has been calculated. Furthermore, the genetic algorithm (GA) is employed for the solution of maximum range of the deflected missile.

1. Introduction

Flight control of missiles is historically realized by tail-fins or canards. Tail-fin controls are located at the rear of the body, well behind the center of gravity. While canard controls are installed in the warhead [1], and are influenced by the head oblique shock. The location of the canards in the expansion region along the nose may result in undesirable aerodynamic and thermodynamic effects occurring in the high dynamic pressure environment [2].

In 1946, Goddard proposed another control device, the deflectable nose, to control missile flight [3]. Through the changing of angles between the missile nose and the body axis, the deflectable nose missile can generate the required control force by air. It has the advantages of simple structure, small additional resistance, little influence on the flow field of tail and high maneuverability. NASA performed wind tunnel tests on missiles with deflectable nose control [4,5] and investigated the feasibility of bent-nose conic shapes as hypersonic aerocapture vehicles for planetary missions [6]. Current studies on the deflectable nose missile are most concentrated in aerodynamic characteristics and dynamic control. Through controlling the head angle of attack, Liang achieved the goals of real-time correction of the trajectory and improved its hitting precision [7]. Gao et al. established a control system based on the concept of deflectable nose and verified its efficiency in hypervelocity flight [8]. Wang et al., based on N-S equation and k-ε turbulent model, simulated the aerodynamic characteristics of models at different angles of attack and Mach numbers, and found that, for low angles of attack, the lift to drag ratio increases with the increase of the angles of attack [9].

Based on previous research, in this paper, we firstly simulates the flow fields of the missile with the deflection angles among 0°–8°, angles of attack from 0° to 8°, and the Mach number from 2 to 5. Then, the aerodynamic forces are calculated based on the numerical results, and are applied to the plumb plane ballistic equations to investigate the flight stability of the deflectable nose missile. Finally GA is adopted to obtain the maximum range.

2. Numerical methods

2.1. Simulation method

Governing equations employed in this paper is Navier-Stokes equations, as shown below

$$\frac{\partial \mu_i}{\partial t} + \mu_j \frac{\partial \mu_i}{\partial x_j} = -\frac{1}{\rho}\frac{\partial p}{\partial x_i} + \upsilon \frac{\partial^2 \mu_i}{\partial x_j \partial x_i} + f_i$$

* Corresponding author.
E-mail addresses: Zhangzhi900720@163.com (Z.-y. Zhang), tang_qz@163.com (Q.-z. Tang), huizi123717@163.com (X.-h. Sun), chenzh@njust.edu.cn (Z.-h. Chen).
Peer review under responsibility of China Ordnance Society.

http://dx.doi.org/10.1016/j.dt.2017.05.001

$$\frac{\partial u_i}{\partial x_i} = 0$$

Since the resistance of missiles caused by the gas viscosity increase at supersonic speeds [10], the surface boundary layer is necessary to be considered in numerical calculation. Large eddy simulation (LES) and direct numerical simulation (DNS) can accurately describe the flow structure of missile. But on the boundary layer, the demand for the grid number and the amount of calculation are relatively large. Reynolds average Navier-Stockes (RANS) has less amount of calculation but cannot accurately simulate the transient flow of turbulence. Therefore detached eddy simulation (DES) is adopted, which uses the RANS for approaching the boundary layer to reduce the demand for the grid number and LES is for the main flow.

In order to effectively catch shock waves near the warhead and tail, two-order AUSM scheme is employed to discrete the convection term. In computational fluid equations, two-order center scheme is used for viscosity term and third-order Runge-Kutta method is employed to discrete the time derivative terms.

The plumb plane ballistic equations are employed for the description of flight of the deflected missile and the 4th-order Runge-Kutta method is adopted for the solution. In the flight calculation, the earth is considered as a still sphere and standard atmosphere model has been adopted. The aerodynamic forces and moments of the plumb plane equations are inputted from the DES simulation.

2.2. Computational model

As shown in Fig. 1, the computational model is a typical three-dimensional deflectable nose missile (N2dB28F240) [11] with the mass of 15.87 kg, diameter of 56.2356 mm.

Fig. 2 displays grid partition in x axis section near the tail. O-Block is built and refined near the boundary layer, and the grid nodes become sparse sequently with its increased distance from the wall. Finally, the number of computational grids is about three million after the gird convergence tests. In addition, the left boundary is considered as the incoming flow and all other boundaries are outflow pressure field and the missile surface is considered as nonslip. The details are seen in the reference [10].

3. Results and discussions

Based on the requirement of parameters for solving the plumb plane ballistic equations, the flow fields of a missile, with the deflection angle varying among $\beta = 0°–8°$, angles of attack, $\alpha = 0°–8°$, and the Mach numbers $Ma = 2–5$, have been simulated numerically.

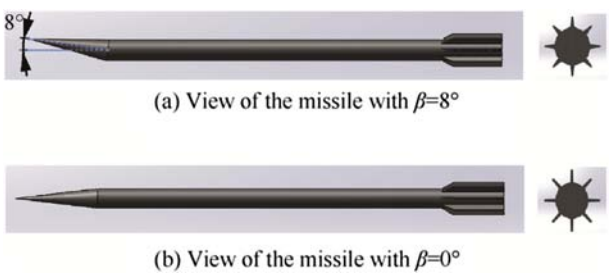

(a) View of the missile with β=8°

(b) View of the missile with β=0°

Fig. 1. Model of the three dimensional deflected nose missile.

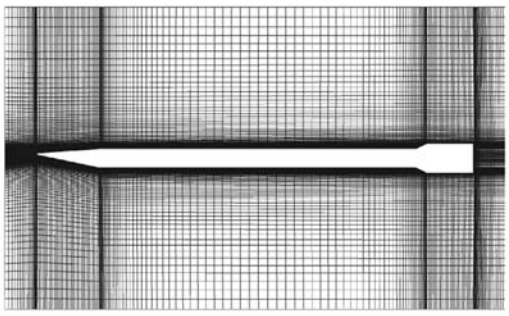

(a) View of the missile-tail mesh in the longitudinal direction

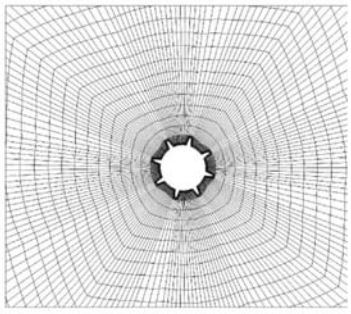

(b) View of the missile-tail mesh in the cross section of x axis

Fig. 2. Mesh of the missile.

3.1. Aerodynamic characteristics of the deflection missile

Fig. 3 presents the typical pressure contours on the surface and around the missile, at angle of attack $\alpha = 0°$ and nose deflection angle of $\beta = 0°$, 4° and 8°, respectively. It is nondimensionalized with the characteristic value of the pressure $P_0 = 73429.16$ pa. It can clearly be seen that, for the case of (a) $\alpha = 0°$, $\beta = 0°$, the flow field structure is almost symmetrical with respect to the axis of missile. At the nose, the oblique shock appears, and the pressure increases significantly around the head and decreases rapidly just behind the shoulder due to the expansion waves. In the middle of the missile there are no shock and expansion waves. The pressure is basically stable. But at the front of the tail, the flow is strongly compressed due to the block of tail foils, and strong oblique shock waves appear, however, there is a low pressure recirculation region at the bottom of the missile.

For the cases of (b) $\beta = 4°$ and (c) $\beta = 8°$, the structure of the flow field is not symmetrical about the XZ plane. The strength of the shock wave on the windward is much higher than that on the leeward, on the contrary, the expansion wave near the shoulder is much weakened on the windward (Fig. 3(b–c)). This is because when the nose deflects upward, the compression of the flow on the windward is enhanced and the turning angle around the shoulder increases to make the flow expand quicker than that of the leeward. The structure of the flow field in the rear of the missile is almost the same for all the cases, but the intensity of the oblique shock of tail foils (Fig. 3(b–c)) is weaker than the non deflectable case (Fig. 3(a)), therefore, the induced drag is smaller.

The high pressure region formed below the nose causes an additional lift over the forebody surface and makes the pressure center move forward, and also a change in aerodynamic coefficients. Fig. 4 exhibits the relationship between aerodynamic coefficients of the missile and angle of attacks, in which the solid line represents numerical simulation values and the dotted line

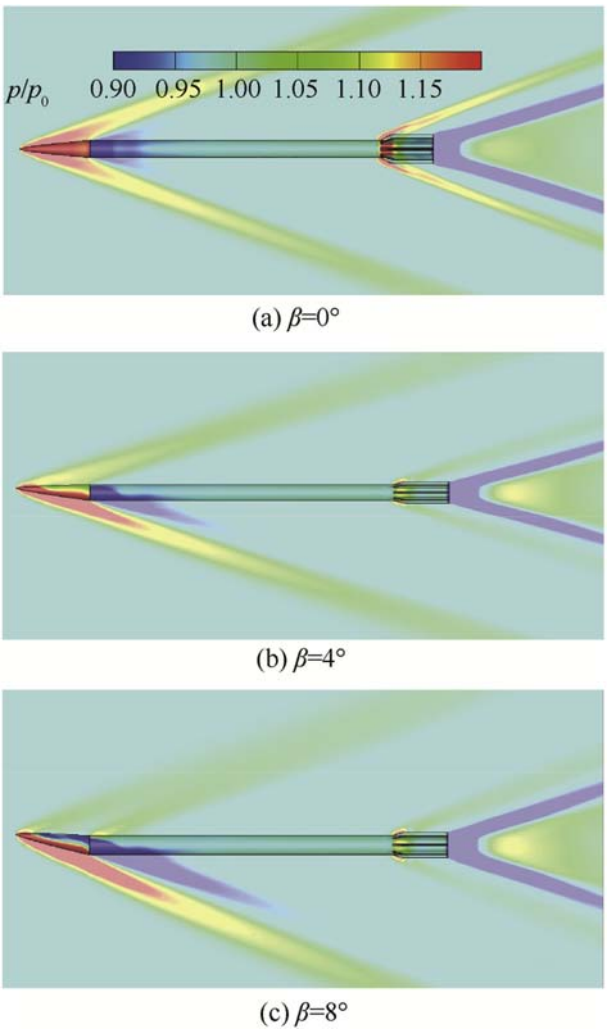

Fig. 3. Pressure conours of a deflectable missiles at $Ma = 3.0$, $\alpha = 0°$ and different deflection angles $\beta = 0°$, 4° and 8°.

indicates the experimental values of Ref. [2]. It is clear that both experimental and numerical results agree well with each other. The drag and lift coefficients increase with the increase of angle of attack and the deflection angle, but the increase gradient of lift is larger. This is because the deflected nose makes the pressure on the windward side increases while that on the leeward side decreases (Fig. 3). The pressure difference causes the increase of the force projected on both x and y axes. The main reason of the extended range of the deflected nose missile is caused by its pitching moment coefficient.

On the other hand, with the increase of attack of angle, the pitching moment decreases and becomes negative at some points, it shows that the missile is longitudinally stable during flight. But for large attack of angles and the deflection angles, the differences between lift coefficients of experiments and numerical simulation become large (Fig. 4(b)), therefore, in this paper, the attack of angles during flight should be kept smaller than 8°.

Fig. 5 illustrates the relationship between aerodynamic coefficients of the missile and Mach number with the nose deflection $\beta = 4°$, angle of attack $\alpha = 0°$, 4°, and 8°. It can be seen that, for supersonic flow, with the increase of Mach number, the drag coefficient decreases, the lift is basically stable. The pitching moment increases slowly for $\alpha = 0°$, 4°, and the smaller its attack of angle,

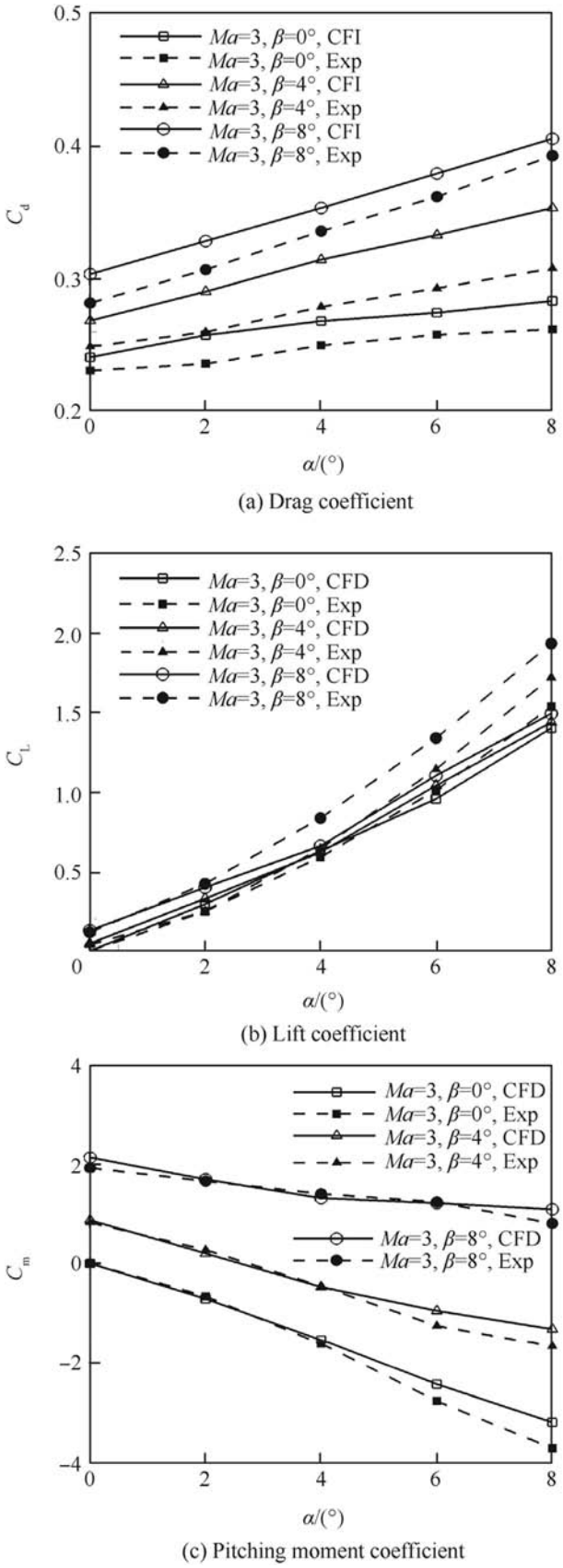

Fig. 4. Comparison of experimental aerodynamic coefficients [2] with our numerical results under $Ma = 3$ and attack of angles.

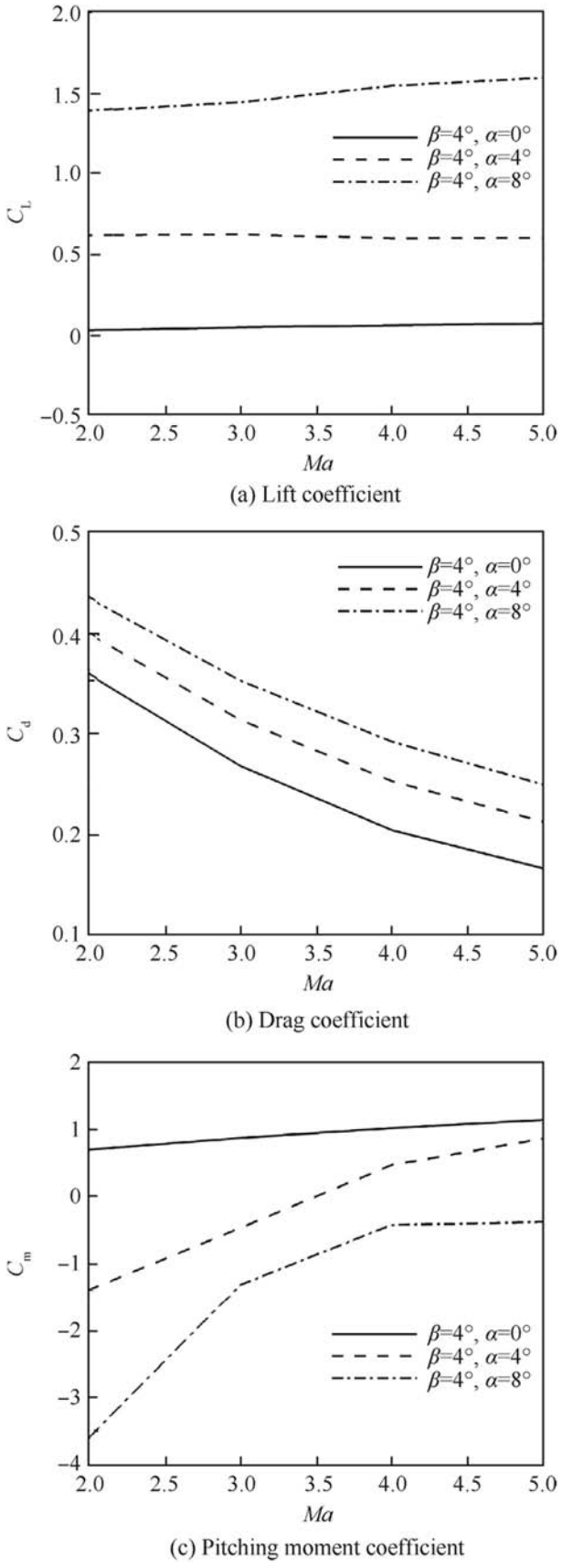

Fig. 5. Aerodynamic coefficients of the missile with $\beta = 4°$ and different mach numbers.

Table 1
Landing state of deflected missile with different deflection angle.

Deflection angle/(°)	*Ma*	Range/m	Pitch angle/(°)
0	2.479	154931	53.61
1	2.478	156598	47.50
2	2.459	158115	42.52
3	2.390	159970	38.27
4	2.254	163463	31.41
5	1.355	182465	20.37

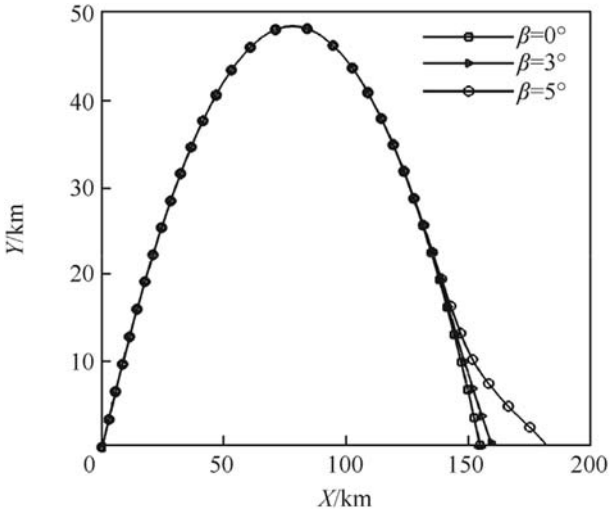

Fig. 6. Trajectory of deflected missile with different deflection angle.

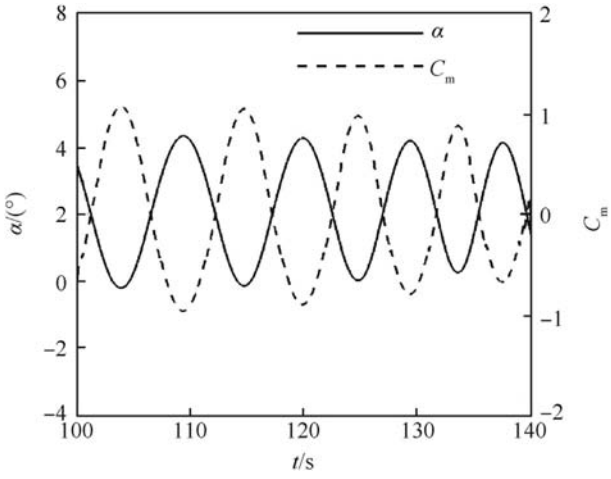

Fig. 7. Time histories of both of the angle of attack and pitching moment coefficient.

the larger its value.

3.2. Trajectory optimization of the deflected nose missile

To simulate the flight trajectory, we take above deflected nose missile as the example. Substitute the calculated aerodynamic coefficients into the 6 DOF ballistic equations to simulate the trajectories of the missile numerically with different deflection angles. We set the deflection starts at the end point of the boost phase, at this time, $t \approx 100$s, the body velocity is 1689 m/s, pitch angle is about 50° and angle of attack is almost zero.

Table 1 displays the landing state of deflected missile after

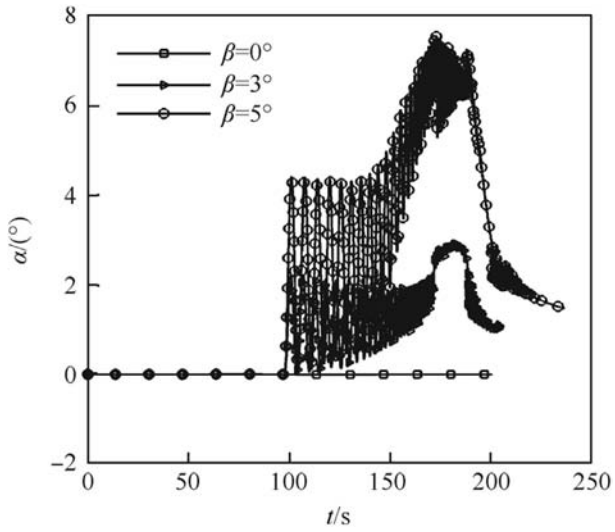

Fig. 8. Curves of attack angle with deflection angle $\beta = 0°$, 3° and 5°.

deflecting the nose at the highest point of the trajectory. Fig. 6 is the missile trajectory with different deflection angles $\beta = 0°$, 3° and 5°. By comparison it is found the range increases progressively with the increase of deflection angle β. When $\beta = 5°$, the growth rate is significantly increased. It illustrates the deflectable nose control can significantly enhance the range of the missile but the landing Mach number and pitch angle both decrease. In addition, if β is over 6°, the angle of attack will exceed 8°. Therefore this condition will not be considered.

Typical profiles of angle of attack and pitching moment coefficient are displayed in Fig. 7. It is clear that the variation of pitching moment is opposite to that of the angle of attack, and acts as the righting moment and keeps the body stable. When the angle of attack increases, the pitching moment decreases, they reach at the extremum values at the same time, then, they vary contrarily again. Both the angle of attack and pitching moment have the same oscillation cycle.

Figs. 8 and 9 shows the curves of attack of angle and lift-to-drag ratio during the flight with different deflection angle $\beta = 0°$, 3° and 5°. It is clear that both attack of angle and lift-to-drag ratio have the same variation tendency with different deflection angles. When $\beta = 0°$, the lift-to-drag ratio are almost equal to 0° during all the flight due to the very small angles of attack. When $\beta = 3°$ or 5°, after the highest point of trajectory, the angle of attack is greater than 0° and the lift coefficient increases. From Fig. 9, the lift-to-drag ratios of the deflected nose missile are large. This is why the range of deflected nose missile is longer than that of normal missile.

However, the deflected nose makes the pressure center move forward with the increased fluctuation of angle of attack and leads to the decrease of flight stability.

We use the projection of overload to the velocity coordinate system (Ox_3y_3) to discuss the overload. Nx_3 is the tangential overload and Ny_3 refers to the normal overload. In fact, a large tangential overload means a large tangential acceleration and the velocity of the missile is changed quickly. Moreover, if the missile has a large normal overload, it is quicker to modify the direction of the flight. Therefore, the larger the overload of the missile is, the better its maneuverability becomes. As displayed in Fig. 10, with the increase of the deflection angle, the tangential overload decreases, but its normal overload increases. Since the growth rate of the

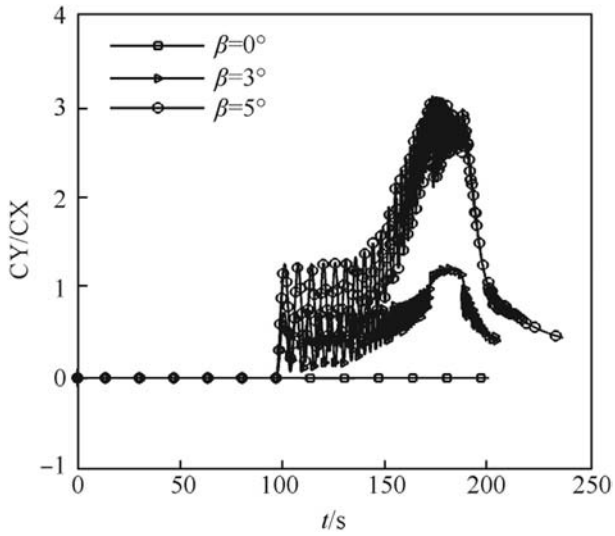

Fig. 9. Curves of lift-drag ratio with deflection angle $\beta = 0°$, 3° and 5°.

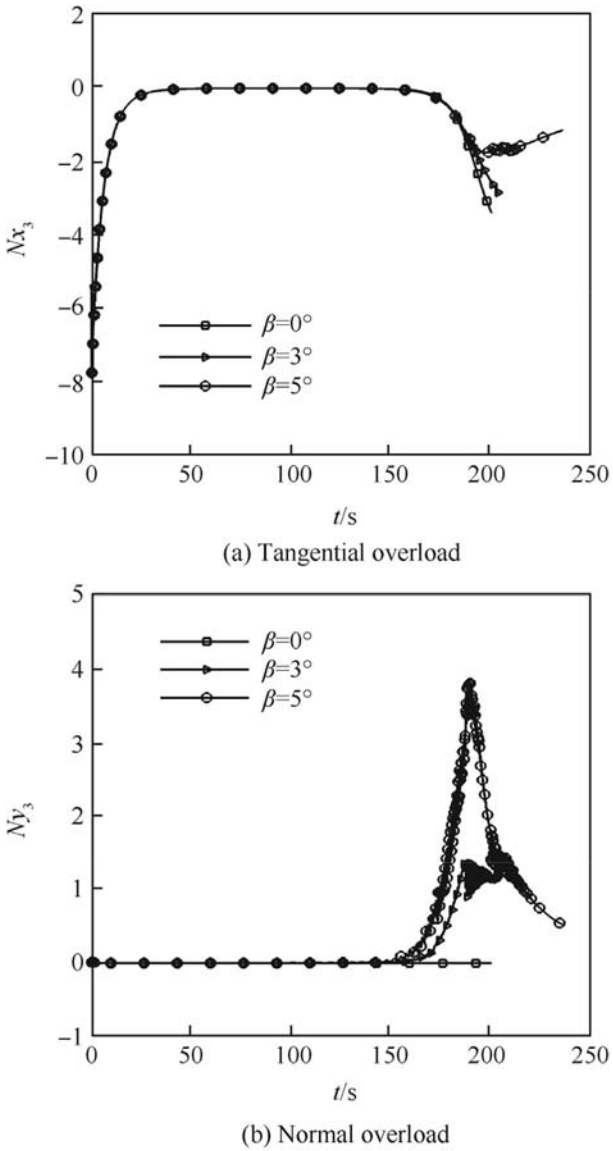

Fig. 10. The projection of overload to the velocity coordinate system.

Table 2
Results of the optimization.

Missile	launch angle/(°)	Deflection time/s	Deflection angle/(°)	Fitness value	Range/m
Normal	52.592	/	/	1.275	156863
Deflected	51.990	103.067	4.915	1.048	190840

normal overload is far larger than the reduction rate of the tangential overload, the deflected missile has better maneuverability.

To investigate the superiority of the deflected missile, two cases, the normal and the deflected missiles, are considered to optimize its trajectory. The former is to search an optimal launch angle for a maximum range. The latter is to search the optimal launch angle and the variation of deflecting angle with time to maximize the range. Since the relationship between objective function and variables is nonlinear, and the objective function is discontinuous, an optimization algorithm which can adapt to the nonlinearity and discontinuity is needed.

Genetic algorithm is ideal for the optimization of our range problems and as it is a probabilistic search algorithm, each case is calculated 5 times to achieve the minimum fitness value as expressed in Eq. (1), where R is the range of the missile. In addition, the population size and the number of generations are taken to be 50 and 500, respectively. And the cross-over probability and mutation probability are chosen to be 0.7 and 0.1, respectively.

$$F_1(\mathbf{x}) = \frac{200000}{R}, \tag{1}$$

Table 2 shows the results of optimization. The range of deflected missile increases from 156863m to 190840m, its extended range is 21.66% higher than that of the normal missile, therefore, the deflected nose missile is obviously advantageous in extending the flight range.

4. Conclusions

By combining computational fluid dynamics and plumb plane ballistic motion equations, the aerodynamic characteristics, extended range and maneuverability of a deflected missile are investigated. The optimized ranges of both normal and deflected missiles are obtained with the use of genetic algorithm. Following conclusions are concluded.

1) The coupling of DES and plumb plane ballistic equations can be used to investigate numerically the flow characteristics and aerodynamic forces of the supersonic deflected missiles.
2) The deflected missile has larger lift, drag and pitching moment coefficients, but the pressure center moves forward, therefore its flight stability is decreased. With the increase of the deflected angle, its ability to change the flight direction is obviously improved.
3) The deflected missile flies at high angle of attack with its lift-to-drag ratio far larger than that of the normal missile and it has a longer range. Through the genetic algorithm, the deflectable nose control can make the maximum range increase 21.66%.

References

[1] Hemidi A, Henry F, Leclaire S, et al. CFD analysis of a supersonic air ejector. Part I: experimental validation of single-phase and two-phase operation. Appl Therm Eng 2009;29(8):1523–31.
[2] Landers MG, Hall LH, Auman LM, et al. Deflectable nose and canard controls for a fin-stabilized missile at supersonic and hypersonic speeds. AIAA 2003. 3805.
[3] Goddard, Robert H. “Apparatus for steering aircraft.” U.S. Patent No. 2,594,766. 29 Apr. 1952.
[4] Winovich W, Higdon N S. Evaluation of Some Aerodynamic Controls for a Low-Aspect-Ratio Missile [J]. NACA RM A58D17b, 1958.
[5] Riley D R. Some effects of nose deflection and number of tail fins on the aerodynamic characteristics in pitch and sideslip of a wingless missile at a Mach number of 3.11 [J]. NASA TM X-270, 1960.
[6] Miller III CG, Gnoffo PA. Pressure distributions and shock shapes for a bent-nose biconic at incidence. AIAA J 1982;20(8):1150–2.
[7] Liang Z. The exterior ballistic study of trajectory correction shell with controlled angle of attack at the shell head. J North China Inst Technol 2001;22(6):403–7.
[8] Yuan Gao, Liangxian Gu, Chunlin Gong. Investigation in a deflectable nose control scheme. J Missiles, Rockets, Missiles Guid 2006;26(1):890–2.
[9] Fei Wang, Guo-dong Wu, Zhi-jun Wang, et al. Numerical calculation of aerodynamic characteristics of shell with attack angle at the shell head. J North China Inst Technol 2005;26(3):177–9.
[10] Yu-jie Guo, Zhi-hua Chen, Jun-li Han. The flow fields and aerodynamic characteristics of the deflected nose missile at different angles of attack. J Aerosp Power 2014;29(9):2079–84.
[11] Shoesmith B, Birch T, Mifsud M, et al. CFD analysis of a supersonic missile with deflectable nose control[C]//Proceedings of the 2003 AIAA 3rd Flow Control Conference. San Francisco: AIAA. 2006, 3200.